Applied Catalysis B: Environmental 239 (2018) 644–653

Contents lists available at ScienceDirect

Applied Catalysis B: Environmental

journal homepage: www.elsevier.com/locate/apcatb

Facile production of biofuel via solvent-free deoxygenation of oleic acid using a CoMo catalyst

Jae-Oh Shim[a], Kyung-Won Jeon[a], Won-Jun Jang[a], Hyun-Suk Na[a], Jae-Wan Cho[a], Hak-Min Kim[a], Yeol-Lim Lee[a], Dae-Woon Jeong[b,*], Hyun-Seog Roh[a,*], Chang Hyun Ko[c,*]

[a] Department of Environmental Engineering, Yonsei University, 1 Yonseidae-gil, Wonju, Gangwon, 26493, Republic of Korea
[b] School of Civil, Environmental and Chemical Engineering, Changwon National University, 20 Changwondaehak-ro, Changwon, Gyeongnam, 51140, Republic of Korea
[c] School of Applied Chemical Engineering, Chonnam National University, 77 Yongbong-ro, Gwangju, 61186, Republic of Korea

ARTICLE INFO

Keywords:
Cobalt molybdenum
Solvent-free
Deoxygenation
Fuel properties

ABSTRACT

Support- and sulfide-free cobalt molybdenum catalysts are prepared via different synthetic procedures for catalytic deoxygenation of oleic acid under inert (N_2) and solvent-free conditions. Among the tested catalysts, the CoMo catalyst prepared via a sol-gel method achieves the highest catalytic performance, namely, 88.9% oleic acid conversion, with 48.1% C_9–C_{17} selectivity, and 69.6% oxygen removal rate, owing to its excellent physical properties. Additionally, oxygen vacancy is formed in CoMo catalyst during sol-gel synthesis process and it also effect on the catalytic activity. Examination of the deoxygenation reaction over pre-reduced catalysts reveals that the $CoMoO_4$ species is the active species in the CoMo catalysts. The fuel properties of the resultant products are affected strongly by the catalytic performances of the CoMo catalysts. The biofuel produced using the CoMo catalyst prepared via the sol-gel method showed the highest calorific value (10,119 cal/g) and the lowest viscosity (31.5 cP), and, consequently, this CoMo catalyst exhibits the highest catalytic activity and has significant potential for application in biofuel production.

1. Introduction

Fatty acid methyl esters (FAMEs), which are known as the first generation bio-diesel, are generally expressed using the chemical formula $RCOOCH_3$ [1–3]. FAMEs are usually synthesized from triglycerides by transesterification with methanol [4]. FAMEs, as suggested by the chemical formula, contain a large amount of oxygen, which leads to thermal instability, corrosiveness, low heating value, and poor flow at low temperatures [3–11]. In particular, triglycerides have olefinic double bonds, which is the reason for the thermal and oxidation instabilities of FAMEs [12]. As a result of the many drawbacks associated with the first-generation bio-diesel, the production of second-generation biofuel has attracted significant attention in recent years [13–15]. The second-generation biofuel can be produced by the deoxygenation of fatty acids. [16–20]. In the recent past various metal catalysts, such as Pd-, Pt-, and Ni-based catalysts, have been applied for deoxygenation reactions [3,5,10,16,17,21–36]. Among them, Pd-based catalysts exhibit the best catalytic activity in deoxygenation reactions [37,38]. Murzin and co-workers revealed that the catalytic activity of monometallic catalysts with various active metals decreases in the following order: Pd > Pt > Ni > Rh > Ir > Ru > Os [17]. However, noble metal-based catalysts could significantly raise the cost of deoxygenation processing [39]. Other approaches involve the use of bimetallic Al_2O_3-supported catalysts in sulfide forms ($NiMoS/Al_2O_3$ and $CoMoS/Al_2O_3$) for deoxygenation reactions [40–42]. However, they have many drawbacks, such as rapid deactivation by coke deposition and a need for the addition of sulfur donor compounds (H_2S, low sulfur content in bio-feedstock) [29,43]. In our previous study, we developed support- and sulfide-free CoMo catalysts for the decarboxylation of oleic acid in H_2-free environment [44]. The Co/Mo ratio of the developed catalysts was optimized (1:1, mole percent) to obtain high catalytic performance [44]. The optimized CoMo catalyst exhibited both high oleic acid conversion and high selectivity for C_{17} hydrocarbons. Although many studies utilizing Al_2O_3-supported sulfide CoMo catalysts for hydordeoxygenation have been reported [45], the catalytic performance of sulfide- and support-free CoMo catalysts in deoxygenation under H_2-free conditions has not been investigated to date. Moreover, detailed optimization of parameters such as the catalyst preparation method has also not been investigated. It is well known that the catalyst preparation method can exert significant influence on the basic physical properties of a catalyst, which in turn influence its catalytic activity.

The oxygen in fatty acids can be eliminated via three main types of

* Corresponding authors.
E-mail addresses: dwjeong@changwon.ac.kr (D.-W. Jeong), hsroh@yonsei.ac.kr (H.-S. Roh), chko@jnu.ac.kr (C.H. Ko).

https://doi.org/10.1016/j.apcatb.2018.08.057
Received 4 June 2018; Received in revised form 28 July 2018; Accepted 22 August 2018
Available online 24 August 2018
0926-3373/

reaction pathways: 1) hydrodeoxygenation, 2) decarboxylation, and 3) decarbonylation [46–49]. With the exception of the hydrodeoxygenation reaction, these reaction pathways do not require a supply of hydrogen as an essential reactant [16,46,50,51]. Recent studies have revealed that the presence of H_2 can affect the selectivity of the decarboxylation and decarbonylation reactions; nevertheless, the use of large quantities of H_2 can significantly increase the total cost of processing [16,50,52]. Thus, we investigated decarboxylation and decarbonylation reactions under H_2-free conditions in order to minimize the consumption of H_2.

The majority of deoxygenation reactions reported in the literature are undertaken in different solvents such as water, dodecane, and toluene [53,54]. However, employing a solvent can cause a significant increase in the processing costs when considered at industrial scale [53]. Moreover, the need for additional separation in the solvent-based systems adds further complications. To date, only few studies have conducted the deoxygenation reaction under solvent-free conditions [5,44,53–55].

We envisaged that deoxygenation reaction under solvent-free conditions could be used to produce biofuel for diesel engines. In addition, it would also make the biofuel for diesel engines production process more facile and easily accessible. Therefore, in the present work, we design and investigate CoMo catalysts for the deoxygenation reaction under solvent-free conditions. In particular, the main objective of this work is to study the effects of the catalyst preparation conditions on the catalytic performance of sulfide- and support-free CoMo catalysts for the deoxygenation reaction under solvent- and H_2-free conditions. For the optimization of the catalyst preparation method, we investigate the incipient wet impregnation synthesis method (CoMo-IWI), co-precipitation synthesis method (CoMo-CP), hydrothermal synthesis method (CoMo-HT), and the sol-gel synthesis method (CoMo-SG). Oleic acid is chosen as the biofuel precursor. We also determine the active species in the CoMo-driven catalytic transformation and analyze the basic fuel properties of the resultant products.

2. Experimental

2.1. Catalyst preparation

CoMo catalysts were prepared by CP (CoMo-CP), IWI (CoMo-IWI), HT (CoMo-HT), and SG (CoMo-SG). A constant Co/Mo molar ratio of 1:1 was applied [44]. The CoMo-CP catalyst was obtained from well-mixed $(NH_4)_6Mo_7O_{24}{\cdot}4H_2O$ (99%, Fluka) and $Co(NO_3)_2{\cdot}6H_2O$ (98%, Aldrich) water solutions by the addition the 28.8% ammonium hydroxide solution at 80 °C. After aging for 4 h, the sample was thoroughly washed with 2 L of distilled water in order to remove any impurities, and air-dried for 12 h, followed by drying at 110 °C. In the case of the CoMo-IWI catalyst, cobalt oxide was first prepared using a precipitation method, with 15-wt% KOH solution as the precipitating agent. Co $(NO_3)_2{\cdot}6H_2O$ (98%, Aldrich) precursor was dissolved in distilled water. The precipitate was aged at 80 °C for 3 days before it was washed five times with distilled water and air-dried for 1 day at 110 °C. The as-dried precipitate (cobalt oxide) was calcined in air from room temperature to 700 °C at a heating rate of 1 °C/min, and the temperature was maintained for 6 h. Next, molybdenum was loaded onto the prepared cobalt oxide, and this catalyst was again calcined at 700 °C for 6 h. The CoMo-HT catalyst was prepared by the hydrothermal method. The metal precursors were dissolved in 120 mL of distilled water. Subsequently, 28.8% ammonium hydroxide solution was added at 80 °C. The solution was treated for 5 h at 150 °C in a hydrothermal reactor. After the hydrothermal treatment, the product was washed with distilled water and dried at 100 °C for 12 h. The fine powder was subsequently calcined at 700 °C for 6 h in air. The CoMo-SG catalyst was prepared by the sol-gel method. The molar ratio of Co/Mo was maintained. Stoichiometric quantities of the cobalt precursor, molybdenum precursor, and citric acid were dissolved in 20 mL of distilled water under stirring. In this reaction, the citric acid served as a chelating agent. After mixing, the solution was kept at 80 °C for 20 h. At this stage, the water was evaporated slowly, resulting in a gel formation as a result of metal complexation with citric acid. Once gel formation was observed, the sample was dried at 100 °C for 4 h in order to afford a fluffy mass via a combustion reaction. The catalyst was calcined at 700 °C for 6 h in air.

2.2. Characterization

The Brunauer–Emmett–Teller (BET) specific surface area of each catalyst was measured using a nitrogen adsorption technique on an ASAP 2010 (Micromeritics) accelerated surface area and porosimetry instrument. Before analysis, the samples were degassed for 12 h at 110 °C under a vacuum < 0.5 mm Hg [56,57]. X-ray diffraction (XRD) measurements were carried out using a Rigaku D/MAX–IIIC diffractometer operated at 40 kV and 100 mA with Ni-filtered Cu − Kα radiation [58]. Transmission electron microscopy (TEM; JEOL JEM-F200) images of the prepared catalysts were obtained at an operating voltage of 200 kV. All samples were suspended in ethanol by ultrasonication. The suspension was deposited on a copper grid for TEM measurements. X-ray photoelectron (XPS) spectra were obtained using a Kα spectrophotometer (VG Multilab 2000) with a high-resolution monochromator. The pressure of the analysis chamber was maintained at 6.8×10^{-9} mbar. The detector was used in the constant energy mode with pass energy of 100 eV for the survey spectrum and 50 eV for the detailed scan. Binding energies were calibrated against the C 1 s transition, which appeared at 284.6 eV [59]. Raman spectra were obtained using a LabRam Aramis (Horiba Jobin Yvon) with excitation at 532 from an Nd-YAG laser. A 500-μm pinhole was used for spectral resolution grating, yielding approximately 1.5 cm^{-1} resolution. Oxygen content was measured by elementary analysis using a Thermo Finnigan FLASH EA-1112 Elemental Analyzer (EA). The oxygen removal efficiency is calculated using the following equations.

$$\textit{Oxygen removal efficiency}\ (\%) = \frac{OC_R - OC_P}{OC_R} \times 100$$

where, OC_R is the oxygen content of oleic acid (11.5) and OC_P is the oxygen content of the product. The calorific value of the product of each deoxygenation reaction was analyzed by Leco AC600 bomb calorimeter instrument using the ASTM D 4809 method. Specifically, 0.5 to 0.8 g of the products was loaded into a tin capsule to analyze the liquid sample. The calorific value measurements were repeated three times and reported as average. The viscosities of commercial diesel, deoxygenation products, and oleic acid were determined at 20 °C with a Brookfield DV 2 T viscometer according to the ASTM D 4878 method.

2.3. Catalytic reaction

Deoxygenation reactions were carried out in an autoclave reactor (100 mL capacity) operating in the batch mode. A multi-blade impeller was installed to mix the solid catalyst and liquid reactant. In a typical batch experiment, 27.5 g of oleic acid and 0.6875 g of catalyst (reactant/catalyst = 40/1, wt%) were placed in the reactor. After oleic acid and the CoMo catalysts were loaded into the reactor, the reactor was flushed with nitrogen to remove any remaining air. The reactor was heated from room temperature to 300 °C at a heating rate of 4.5 °C/min, and the final reaction temperature was maintained for 3 h. The stirring speed was fixed at 300 rpm during the reaction. The reactor was subsequently cooled to room temperature. The liquid products were collected after removal of the solid phase catalysts from the mixture via filtration. The liquid products were analyzed using gas chromatography (HP 6890 N) with a flame ionization detector and a capillary column (HP-5, 30 m). The product gas from the batch reactor was sampled into a 0.5-L Tedlar gas sampling bag (CEL Scientific Corp.) and was analyzed using an online micro-gas chromatograph (Agilent 3000) equipped with molecular sieves and PLOT U columns. In order to identify the active

species, two batches of CoMo-SG catalysts were reduced in 10% H_2/N_2 atmosphere under a pressure of 1 atm at 700 °C (heating rate: 2.9 °C/min) for 2 h. A passivation process using 10% Air/N_2 at room temperature for 12 h followed prior to the exposure of the reduced catalysts to air in order to avoid explosive oxidation. Subsequently, one catalyst was utilized in the original deoxygenation reaction (H_2-free), while the second catalyst was used in a reaction that was performed under 20 bar of pure hydrogen. The conversion of oleic acid and the selectivity of each individual paraffin and olefin C_i products were calculated using the following equations (n : mole of compound, i : carbon number).

$$\textit{Oleic acid conversion}\ (\%) = \frac{n_{\textit{Oleic acid},in} - n_{\textit{Oleic acid},out}}{n_{\textit{Oleic acid},in}} \times 100$$

$$C_i\ \textit{selectivity}\ (\%) = \frac{n_{C_i}}{n_{\textit{Oleic acid},in} - n_{\textit{Oleic acid},out}} \times 100$$

3. Results and discussion

3.1. Catalyst characterization

The BET specific surface areas of the CoMo catalysts prepared using different synthetic methods are listed in Table 1. The BET specific surface area of CoMo-SG is the highest when compared to the other prepared catalysts. Conversely, CoMo-IWI exhibits the lowest BET specific surface area of 2.0 m^2/g. These results indicate that the BET specific surface area of the CoMo catalyst is strongly dependent on the method employed for its preparation. The BET specific surface area of the CoMo catalysts fabricated using the different preparation methods decreased in the following order: CoMo-SG (6.7 m^2/g) > CoMo-CP (4.8 m^2/g) > CoMo-HT (4.5 m^2/g) > CoMo-IWI (2.0 m^2/g). In general, the BET specific surface areas of support-free catalysts are somewhat lower than those of supported catalysts. According to our previous work, the high BET specific surface area of support-free CoMo catalyst enhances their catalytic activity [44].

The XRD patterns of the various CoMo catalysts are presented in Fig. 1. The spectra of all the catalysts exhibit a diffraction peak arising from β-$CoMoO_4$ crystallites [60]. From the XRD results, it is therefore clear that the β-$CoMoO_4$ crystallites are formed regardless of the catalyst preparation method. According to literature reports, $CoMoO_4$ exists in two different phases, generally elucidated as α-$CoMoO_4$ and β-$CoMoO_4$ [60–62]. When the α-phase of $CoMoO_4$ is heated above 650 °C, phase change is initiated, and β-$CoMoO_4$ is completely formed at temperatures about 750 °C. Therefore, the fact that the β-phase of $CoMoO_4$ (marked as $CoMoO_4$) formed in all of the prepared catalysts can be explained by the fact that the tested catalysts were calcined at 700 °C. All the observed reflections of the prepared catalysts could be indexed to monoclinic structure (C2/m space group) [61,63, JCPDS #21-0868]. In order to investigate the crystallinity of each prepared catalyst, Raman spectroscopy analysis was performed and the results are shown in Fig. 2. In Raman spectra, the bands observed around 330, 365, 813, 870, and 936 cm^{-1} are characteristic for $CoMoO_4$ [60,61,64]. Although the peak shapes and intensities differ slightly between the spectra, all spectra contain a $CoMoO_4$ characteristic peak. Thus, all of the prepared catalysts contain $CoMoO_4$ crystallites, irrespective of the synthesis method employed.

Table 1
The characteristics of CoMo catalysts fabricated using different preparation methods.

Catalyst	BET specific surface area (m^2/g)[a]	$CoMoO_4$ average particle size (nm)
CoMo-SG	6.7	31.5
CoMo-IWI	2.0	152.0
CoMo-HT	4.5	137.2
CoMo-CP	4.8	80.4

[a] Estimated from N_2 adsorption at −196 °C.

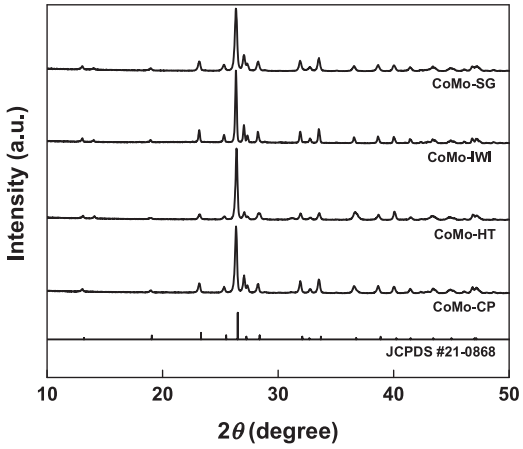

Fig. 1. XRD patterns of CoMo catalysts prepared using different synthetic methods.

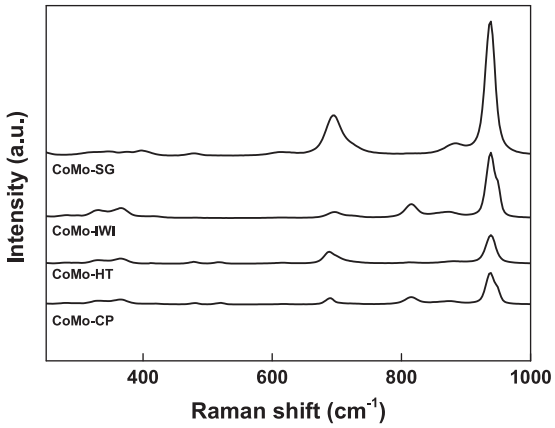

Fig. 2. Raman spectra of CoMo catalysts prepared using different synthetic methods.

Fig. 3 displays the TEM images of the CoMo catalysts prepared using different synthetic methods. The $CoMoO_4$ average particle size was calculated from the TEM images and the results are listed in Table 1. The $CoMoO_4$ average particle size of CoMo-SG is the smallest (31.5 nm) among the prepared catalysts, while that of CoMo-IWI is the largest (152.0 nm). The $CoMoO_4$ average particle size of the CoMo catalysts fabricated using different preparation methods increases in the following order: CoMo-SG (31.5 nm) < CoMo-CP (80.4 nm) < CoMo-HT (137.2 nm) < CoMo-IWI (152.0 nm).

The surface atomic valence states of Co and Mo in the CoMo catalysts prepared using different synthetic procedures were analyzed by XPS measurements. Fig. 4(a) shows the Co 2p spectra of the prepared catalysts. Two peaks are observed around at 780.3 eV and 796.4 eV, which are associated with Co $2p_{3/2}$ and Co $2p_{1/2}$, respectively. All indicated peaks are ascribed to Co^{2+} species in the $CoMoO_4$ phase [65–69]. Fig. 4(b) shows the Mo 3d XPS spectra of the various CoMo catalysts. With the exception for the CoMo-SG catalyst, the spectra clearly contain two distinct peaks at binding energies of 233.0 eV and 236.1 eV, which correspond to Mo $3d_{5/2}$ and Mo $3d_{3/2}$, respectively. These peaks are caused by the two-spin orbit split and are separated by 3.1 eV [65,67]. Interestingly, the Mo 3d XPS spectrum of the CoMo-SG catalyst contains two peaks that have lower binding energies than the peaks in the spectra of the remaining prepared catalysts. The Mo 3d XPS spectrum of the CoMo-SG catalyst fitted well to two 3d doublets in the form of Gaussian function, and these doublets were assigned to the two

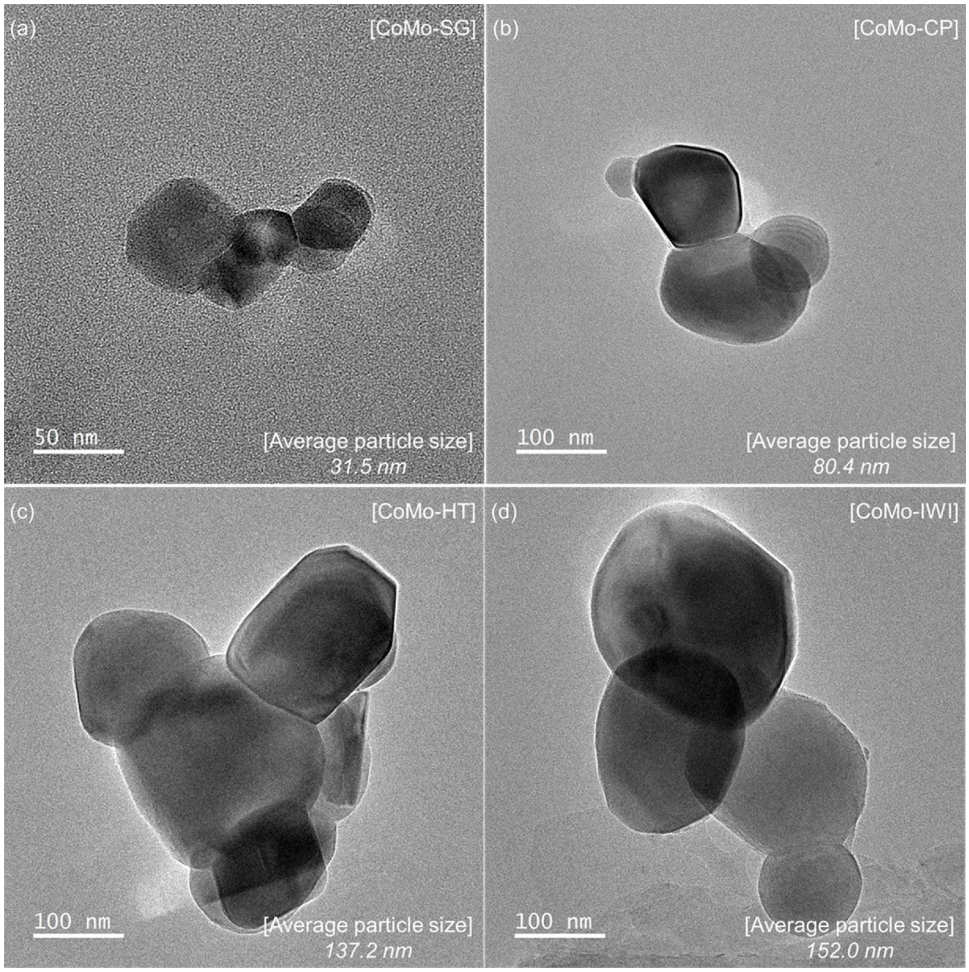

Fig. 3. TEM images of CoMo catalysts prepared using different synthetic methods: (a) CoMo-SG, (b) CoMo-CP, (c) CoMo-HT, (d) CoMo-IWI.

different oxidation states of molybdenum [70–72]. The main peak pair, centered at 231.9 eV and 235.0 eV, was assigned as the 3d doublets of Mo^{5+}. The other peak pair, with peak energies of 233.3 eV and 236.5 eV, corresponds to Mo^{6+} [70–72]. Thus, it can be concluded that oxygen vacancies were formed in the CoMo-SG catalyst [70–72]. The formation of these oxygen vacancies may be caused by the use of citric acid during the catalyst synthesis via the sol-gel process. According to literature, citrate ions play a key role as the reductant species in the sol-gel method [73,74]. Hence, oxygen vacancies were formed in the CoMo-SG catalyst as a result of the reducing nature of citric acid. It should be noted that this special characteristic was maintained despite the additional thermal treatment (calcination of as-prepared catalyst at 700 °C).

3.2. Reaction results

Table 2 displays the results of oleic acid deoxygenation over CoMo catalysts prepared via different synthetic methods. The catalysts exhibited markedly different catalytic performances, confirming thus that the catalytic activity and selectivity were affected by the catalyst preparation method. The CoMo-SG catalyst exhibited the highest oleic acid conversion (88.9%) when compared to the other catalysts. This result clearly shows that the high BET specific surface area (6.7 m^2/g) and small particle size of $CoMoO_4$ (31.5 nm) improve the oleic acid conversion by the CoMo catalyst in the deoxygenation reaction under solvent-free conditions. The low oleic acid conversion of CoMo-IWI is most likely related to its poor physical properties (BET specific surface area: 2.0 m^2/g, $CoMoO_4$ particle size: 152.0 nm). The oleic acid conversion in the presence of the various catalysts decreased in the following order: CoMo-SG (88.9%) > CoMo-CP (87.2%) > CoMo-HT (84.9%) > CoMo-IWI (62.0%). Interestingly, this trend matches well the physical properties of the prepared catalysts as determined by BET and XRD analyses, which implies that the physical properties of the catalysts play a vital role in determining the outcome of the deoxygenation reaction, in which oleic acid is converted to other products. In addition, the formation of oxygen vacancies in CoMo-SG catalysts has beneficial effects on the catalytic performance. Thus, the CoMo-SG catalyst had the best catalytic performance as a result of both its physical properties and oxygen vacancies. The selectivities for linoleic acid, stearic acid, C_{17} hydrocarbons, and C_9 to C_{16} hydrocarbons are listed in Table 2. Arend et al. reported that oleic acids can release one mole of H_2 and produce linoleic acid (di-unsaturated) under inert conditions [50]. The formation of di-unsaturated linoleic acid supplies the hydrogen, which can be used for hydrogenation of oleic acid. The existence of stearic acids further corroborates this phenomenon. When the catalysts had relatively high selectivity for linoleic acid (CoMo-SG and CoMo-IWI), they also had relatively high selectivity for stearic acid. The trend in C_{17} hydrocarbons selectivity appeared to be similar to that in oleic acid conversion. The CoMo-SG (25.5%) exhibited the highest conversion to C_{17} hydrocarbons, and CoMo-IWI (10.6%) the lowest. In addition, the CoMo-SG catalysts exhibited C_9 to C_{16} (diesel fuel range) selectivity that was more than twice as high as those of the other catalysts [3,6]. The excellent catalytic performance of the CoMo-SG catalyst most likely stems from the combined contributions of its physical properties (BET specific surface area and particle size) and its unique chemical properties (oxygen vacancies from Mo^{5+} species), as

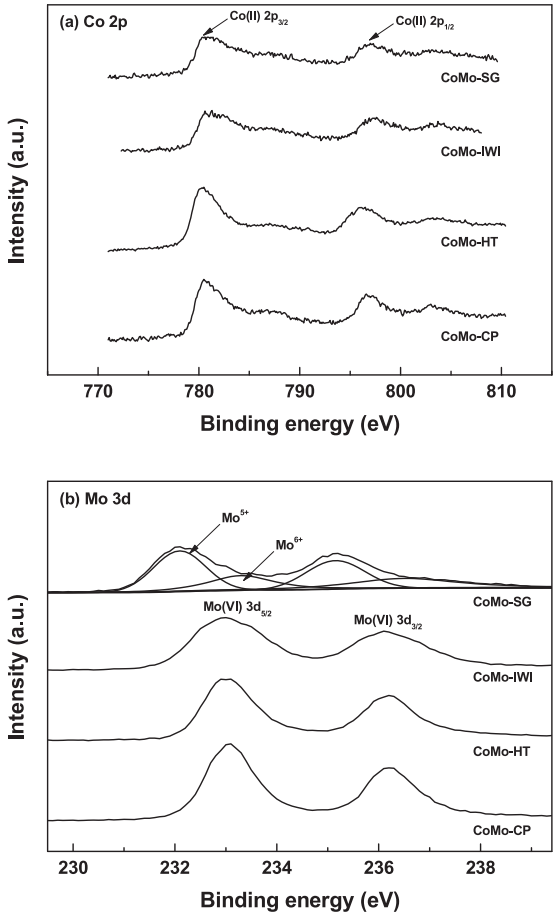

Fig. 4. XPS spectra of CoMo catalysts prepared using different synthetic methods: (a) Co 2p and (b) Mo 3d.

Table 2
Overview of reaction outcomes achieved with CoMo catalysts fabricated using different preparation methods (reaction conditions: 300 °C, reactant/catalyst = 40/1, 1 atm, N_2).

Catalyst	$X_{O.A.}$ [a]	$S_{LO.A.}$ [b]	$S_{S.A.}$ [c]	S_{C17} [d]	$S_{C9–C16}$ [e]	$S_{diesel\ (C9–C17)}$
CoMo-SG	88.9	5.0	7.2	25.5	22.6	48.1
CoMo-IWI	62.0	5.4	7.9	10.6	9.1	19.7
CoMo-HT	84.9	1.1	2.0	13.2	9.6	22.8
CoMo-CP	87.2	2.3	4.2	20.6	10.4	31.0

[a] Conversion of oleic acid (%).
[b] Selectivity for linoleic acid (%).
[c] Selectivity for stearic acid (%).
[d] $S_{C17:1}$ (8-heptadecene, %) + $S_{C17:0}$ (heptadecane, %).
[e] Saturated hydrocarbons + unsaturated hydrocarbons (%).

determined by BET, XRD, and XPS analyses. Literature reports have shown that carboxylic acid groups are first adsorbed at the oxygen vacancy sites, and this process is followed by elimination [75,76]. Thus, the existence of oxygen vacancies in the CoMo-SG catalyst may accelerate the conversion of oleic acid to hydrocarbons. Although the initial conditions of the reaction in this paper were inert (N_2), they changed as the reaction itself generated a small amount of hydrogen. We assume that the solvent-free conditions change the reactor conditions from abundant reactant, which was used to convert oleic acid to stearic acid.

Having established the conversion efficiencies and selectivities of the catalysts, we next investigated the pressure differences as function of time on stream for the CoMo catalysts prepared using different methods (Fig. 5). The initial pressure increased slightly (1 bar → ~6 bar) as the reaction temperature increased to 300 °C. This increase

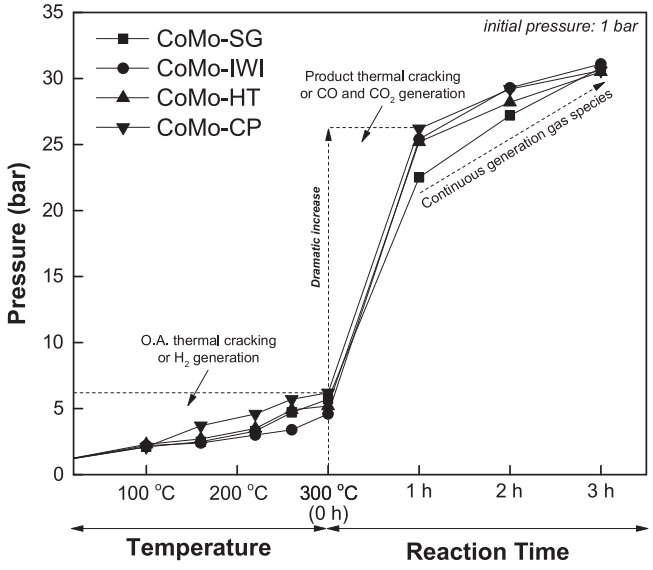

Fig. 5. Pressure differences observed as a function of time on stream in reactions utilizing CoMo catalysts prepared using different synthetic methods.

may be caused by the thermal cracking of oleic acid and the generation of hydrogen. In addition, unsaturated fatty acids are first hydrogenated to saturated fatty acids (i.e., double bond hydrogenation), followed by the deoxygenation of saturated acids to afford hydrocarbons [7]. After the heating was completed, the pressure increased dramatically during the first hour (~6 bar → > 22 bar) as a result of the thermal cracking of products and CO and CO_2 generation by processing decarbonylation and decarboxylation reactions. The pressure also increased gradually as the reaction time increased. Fig. 6 shows the changes in oleic acid conversion, and selectivities for stearic acid, C_{17} hydrocarbons, and C_9–C_{16} as a function of time on stream over the CoMo-SG catalyst. Since the changes in pressure as a function of time on stream of the tested catalysts were similar, we have selected CoMo-SG catalyst, which displays the highest catalytic activity, for further experiments. As the initial reaction temperature reached 300 °C, only a small amount of oleic acid is converted to products. As shown in Fig. 5, oleic acid was thermally cracked and converted to linoleic acid. Interestingly, although the selectivity for stearic acid at t = 0 h was relatively high, it decreased with increasing time on stream (17.2%, 0 h → 7.2%, 3 h). These results indicate that stearic acid was formed before the reaction and was

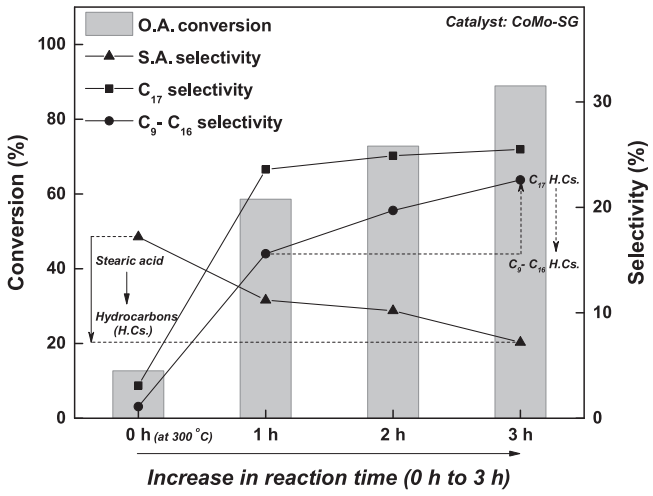

Fig. 6. Changes in oleic acid conversion and selectivities for stearic acid, C_{17} hydrocarbons, and C_9–C_{16} observed as a function of time on stream in reaction utilizing the CoMo-SG catalyst.

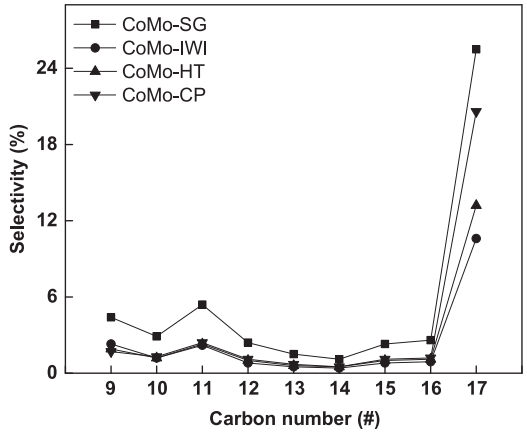

Fig. 7. Distributions of linear hydrocarbons in reaction products afforded using different CoMo catalysts.

decarboxylated/decarbonylated to afford saturated/unsaturated hydrocarbons. Another noteworthy feature of this reaction is that 23.6% C_{17} selectivity was achieved already after 1 h and increased further with increasing reaction time (23.6%, 1 h → 25.5%, 3 h). The C_9–C_{16} selectivity also increased dramatically; however, in this case, it increased proportionally to increasing reaction time (1.1%, 0 h → 15.6%, 1 h → 19.7%, 2 h →22.6%, 3 h). The increase in the selectivity for C_9–C_{16} was caused mainly by the cracking of C_{17} hydrocarbons, which were generated continuously from oleic acid, and were also continuously being cracked to light hydrocarbons.

Fig. 7 shows the distributions of linear hydrocarbons in the total diesel range hydrocarbons (including saturated and unsaturated C_9–C_{17} hydrocarbons) presents in the product pool in reactions employing the various CoMo catalysts. Although the initial selectivity for C_{17} hydrocarbons of each catalyst was different, the trends in the distributions of the linear hydrocarbons were very similar. The differences in the initial C_{17} hydrocarbon selectivities originated from the physical and chemical properties of the catalysts. The diesel fuel range hydrocarbons are derived from the thermal and catalytic cracking of C_{17} hydrocarbons. Thus, it can be said that the cracking properties of the prepared catalysts were fairly similar. In the case of the CoMo-SG catalyst, however, the selectivity for C_9–C_{16} hydrocarbons was almost twice as high as those of the other catalysts. The excellent catalytic performance of the CoMo-SG catalyst is directly linked to its high C_9–C_{16} hydrocarbon selectivity.

Fig. 8 displays the percentages of heptadecane (saturated) and 8-heptadecene (unsaturated) formed in the reaction products as a function of the catalyst. Interestingly, unsaturated 8-heptadecene was

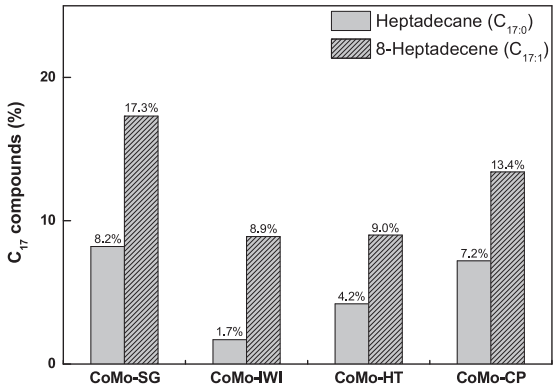

Fig. 8. Percentage of saturated C_{17} hydrocarbon and unsaturated C_{17} hydrocarbon in reaction products obtained in the presence of different CoMo catalysts.

produced more from oleic acid than from saturated heptadecane. This result indicates that decarboxylation is the main reaction pathway in this study. In order to identify the gaseous products formed after the deoxygenation reaction, micro-GC analysis was carried out (Table 3). The analysis revealed that the composition was > 50% of CO_2 for all of the tested catalysts. Carbon dioxide is released by decarboxylation of the carboxyl group (−COO) in fatty acids. CO was detected as the component with the second highest content, and was produced via decarbonylation of fatty acids. These results are in good agreement with the percentages of heptadecane and 8-heptadecene. In addition, N_2 as the residue of purging gas and H_2 were detected in the micro-GC analysis. The existence of a small amount of H_2 corroborates further the above-mentioned reaction step. For the CoMo-HT and CoMo-CP catalysts, the content of CO was relatively low and the content of CH_4 was relatively high. These results can be attributed to the methanation of carbon monoxide. Several other products were also detected in the gaseous product, however their identity could not be determined due to the characteristics of the micro-GC analysis. It is possible that these compounds are shorter hydrocarbons and oxygenated compounds [17,44].

Next, we examined the oxygen removal rates of the prepared catalysts and the oxygen contents remaining in the products (Fig. 9). The presence of oxygen in biofuel can result in thermal instability, corrosiveness, and low heating efficiency [3,5,77–80]. Increasing the efficiency of oxygen elimination is therefore important for improving biofuel quality. Thus, the oxygen removal capacity of a catalyst has direct effect on the fuel properties of the produced biofuel. In the present work, the CoMo-SG catalyst exhibited the highest oxygen removal rate (69.6%) and contained the lowest oxygen content (3.5%). The oxygen removal rates and the remaining oxygen contents of the CoMo catalysts prepared using various synthetic method decreased in the following order: CoMo-SG (69.6%, 3.5%) > CoMo-CP (67.8%, 3.7%) > CoMo-HT (59.1%, 4.7%) > CoMo-IWI (21.7%, 9.0%). It is apparent from these results that the physical and chemical properties of the catalysts were also affecting their oxygen removal properties. Overall, the biofuel for diesel engines produced using the CoMo-SG catalyst is expected to have better fuel properties than those produced using the remaining catalysts.

3.3. Identification of the active species

In order to confirm the nature of the active species in the CoMo-SG catalyst, we carried out the deoxygenation reaction over pre-reduced CoMo-SG catalyst under N_2 (CoMo-SG_R) and pre-reduced CoMo-SG catalyst under 20 bar H_2 (CoMo-SG_R, H_2). The analysis of the reaction progress revealed that the oleic acid conversion and hydrocarbon selectivity decreased rapidly in the case of the reduced CoMo catalyst (Fig. 10). Following the catalyst reduction, the conversion of oleic acid decreased by 30.8% and the C_{17} selectivity by 17.6%. This result clearly shows that $CoMoO_4$ is the active component in the studied reaction. In our previous work, we showed that $CoMoO_4$ species are reduced at around 510 °C [44]. Thus, the small amount of H_2 that is generated in the reaction cannot reduce the CoMo catalyst at 300 °C (i.e., the reaction temperature), thereby allowing the catalyst to retain its activity. Instead, the generated hydrogen is only used in the hydrogenation of oleic acid to produce stearic acid. Analysis of the reduced catalyst in the presence of excess H_2 showed that the catalytic performance of the CoMo catalyst was suppressed—in fact, only the stearic acid selectivity increased in the excess H_2 conditions when compared to the H_2-free conditions.

Scheme 1 shows the possible deoxygenation reaction steps that can take place under inert and solvent-free conditions. In the first temperature rising step, oleic acid is dehydrogenated to linoleic acid. In this process, hydrogen is generated to convert oleic acid. When the heating is complete, oleic acid and the formed stearic acid are decarboxylated and decarbonylated to C_{17} hydrocarbons. As the reaction time increases

Table 3
Results of micro-GC analysis of the products obtained over CoMo catalysts fabricated using different preparation methods.

Catalysts	CH_4 (%)	CO (%)	CO_2 (%)	H_2 (%)	N_2 (%)	Other (%)	Total (%)
CoMo-SG	0.6	26.3	49.8	8.3	6.6	8.4	100.0
CoMo-IWI	1.5	27.6	46.9	7.3	6.8	9.9	100.0
CoMo-HT	8.0	14.8	55.2	6.8	5.4	9.8	100.0
CoMo-CP	6.5	18.2	50.3	7.3	5.7	12.0	100.0

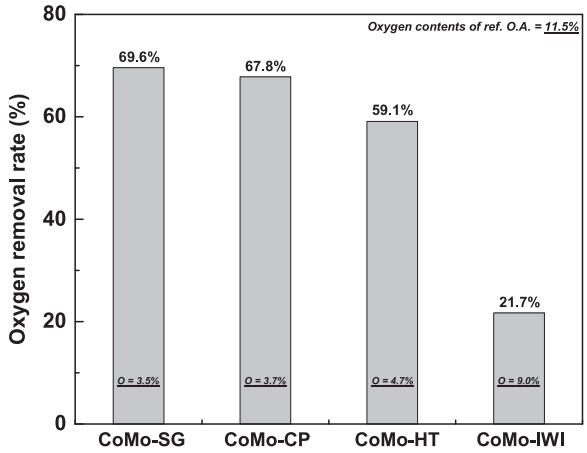

Fig. 9. Oxygen removal rates of the prepared catalysts and the oxygen contents of the corresponding reaction products.

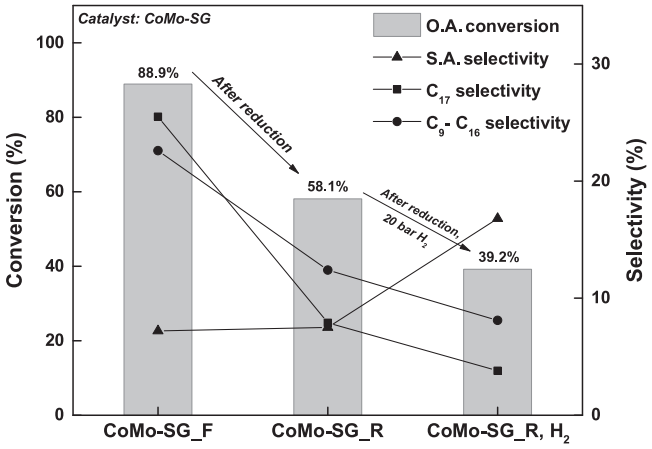

Fig. 10. The results of reactions utilizing fresh and reduced CoMo-SG catalysts under different conditions.

further, the formation and cracking of C_{17} hydrocarbons continuous to occur, generating C_9–C_{16} hydrocarbons.

3.4. Testing the applicability of the biofuel as a diesel fuel

In order to assess the possibility of utilizing the produced biofuel as a diesel fuel, calorific value analysis was carried out. The calorific values of commercial diesel, CoMo catalysts fabricated using different preparation methods, and oleic acid are shown in Fig. 11. Remarkably, the biofuel produced using the CoMo-SG catalyst exhibited a calorific value (10,119 cal/g) that was similar to that of commercial diesel (10,180 cal/g). The calorific value of commercial diesel determined in this work is in good agreement with the reported value (42,940 kJ/kg = 10,258 cal/g) [81–84]. The fact that the CoMo-SG catalyst exhibited the highest calorific value when compared to the other catalysts can be attributed to the fact that the reaction product formed in the presence of CoMo-SG contained the highest content of C_9–C_{17} hydrocarbons and the lowest content of oxygen-containing compounds. For the CoMo-IWI catalyst, its calorific value (7987 cal/g) was only marginally higher than that of oleic acid (7855 cal/g). Literature review reveals that diesel engine performance is influenced by fuel properties such as mass-based calorific value, viscosity, density, and molecular oxygen content [77]. Lower mass-based calorific values are associated with increased fuel consumption, and therefore decreased engine performance. Taking these facts into consideration, out of the examined catalysts, only the CoMo-SG catalyst is suitable for use in diesel engines.

The viscosities and densities of commercial diesel, oleic acid, and the CoMo catalysts prepared via different methods are shown in Fig. 12. Among the various products, the one produced over the CoMo-SG catalyst exhibited the lowest viscosity (31.5 cP). By contrast, the viscosity values of the products afforded using the other CoMo catalysts and oleic acid were all above 7.5 times higher than that of commercial diesel. The biofuel afforded using the CoMo-SG catalyst also displayed higher density (0.929 g/mL) than those produced using the remaining catalysts. In the cases of the biofuel produced using the CoMo-SG and CoMo-CP catalysts, their density increased after the catalytic upgrade process when compared to that of oleic acid. By contrast, the densities of the biofuel afforded using the CoMo-HT and CoMo-IWI catalysts were lower than that of oleic acid. Out earlier work revealed that high viscosity in biofuel can cause poor atomization in the fuel injection process, which affects the air-fuel mixing process and results in incomplete combustion (i.e., production of CO increases) [77,81]. Thus, the poor physical properties of the produced biofuel must be improved by applying an upgrading process.

The physical properties of the catalysts and the reaction outcomes achieved with the catalysts were summarized in order to facilitate comparison, as illustrated in Fig. 13. It is apparent from this comparison that the physical properties of the CoMo catalysts were affected by the method employed for their preparation. In particular, the sol-gel preparation method afforded a catalyst with a beneficial characteristic—namely, the presence of oxygen vacancies. The physicochemical properties, in turn, had a significant effect on the deoxygenation reaction and the composition of the resultant products. The trend in catalytic performance was similar to that in physical properties of the catalysts. Analysis of the comparison shown in Fig. 13 clearly confirms that the results explain the relationships between physicochemical properties and the observed reaction outcomes. Specifically, the fuel properties of the resultant products are strongly dependent on the oleic acid conversion, C_9–C_{17} selectivity (including selectivity for C_{17} only), and oxygen removal rate. Based on this relationship, it can be concluded that high catalytic performance facilitates the formation of a biofuel with a high calorific value and low viscosity. As a result, the CoMo catalyst prepared via the sol-gel method exhibits the highest catalytic activity and the best potential for use in biofuel production. The active species in the CoMo catalyst prepared in this study by the sol-gel method is $CoMoO_4$.

4. Conclusions

In the present work, we showed that the catalytic performance of CoMo catalysts depends strongly on the preparation method. The CoMo catalyst prepared by the sol-gel method converted successfully oleic acid into diesel-range hydrocarbons under inert and solvent-free

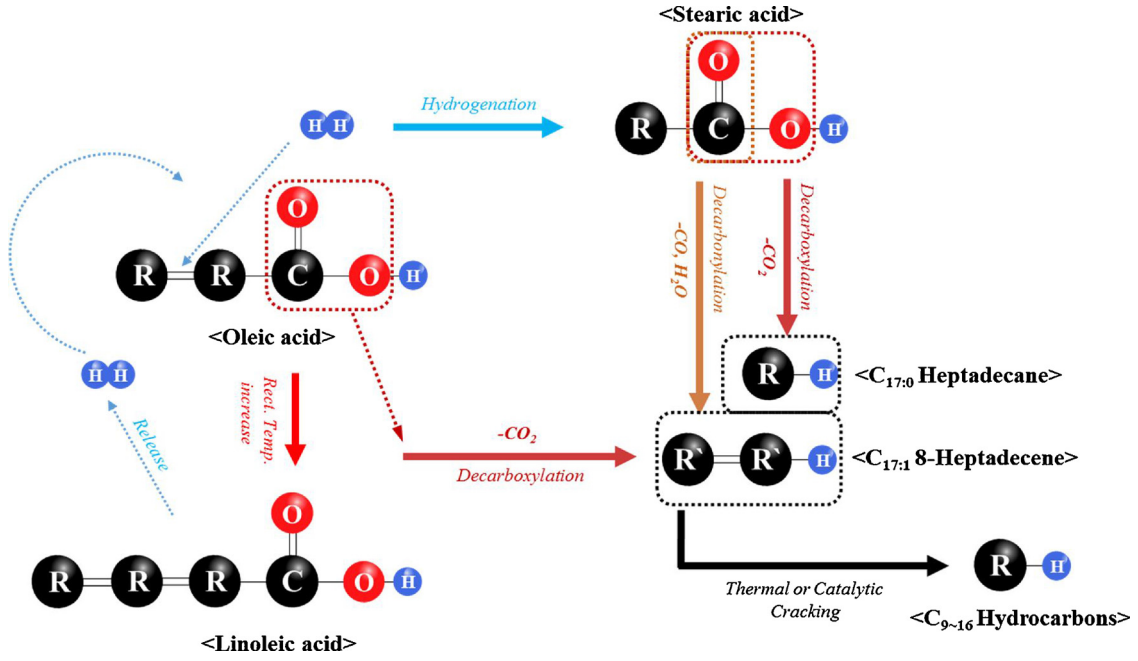

Scheme 1. Potential reaction steps in the deoxygenation pathway under inert and solvent-free conditions.

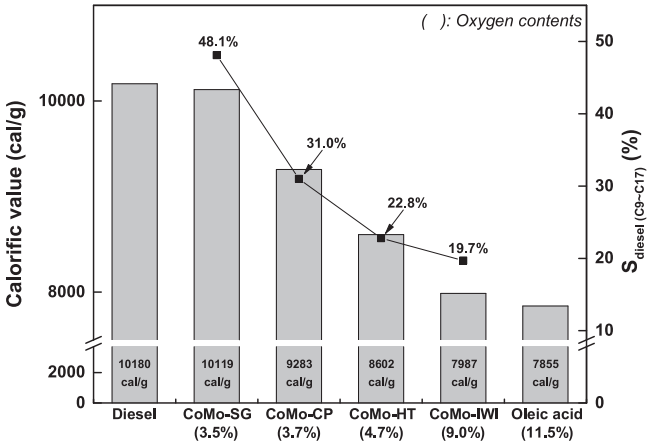

Fig. 11. The calorific values of commercial diesel, CoMo catalysts prepared using different synthetic methods, and oleic acid.

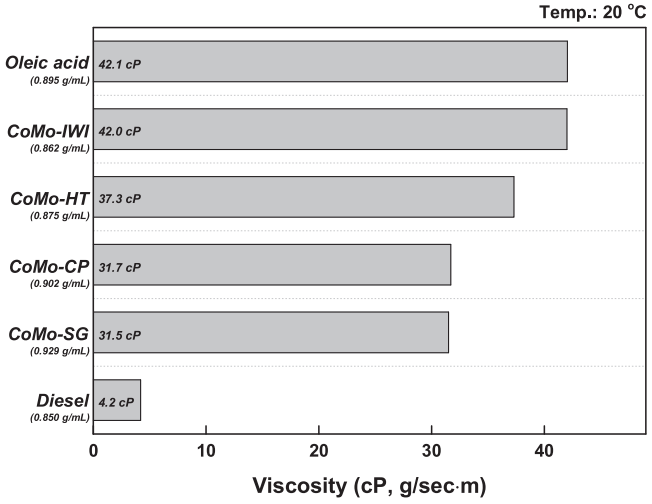

Fig. 12. The viscosity and density values of commercial diesel, oleic acid, and CoMo catalysts prepared using different synthetic methods.

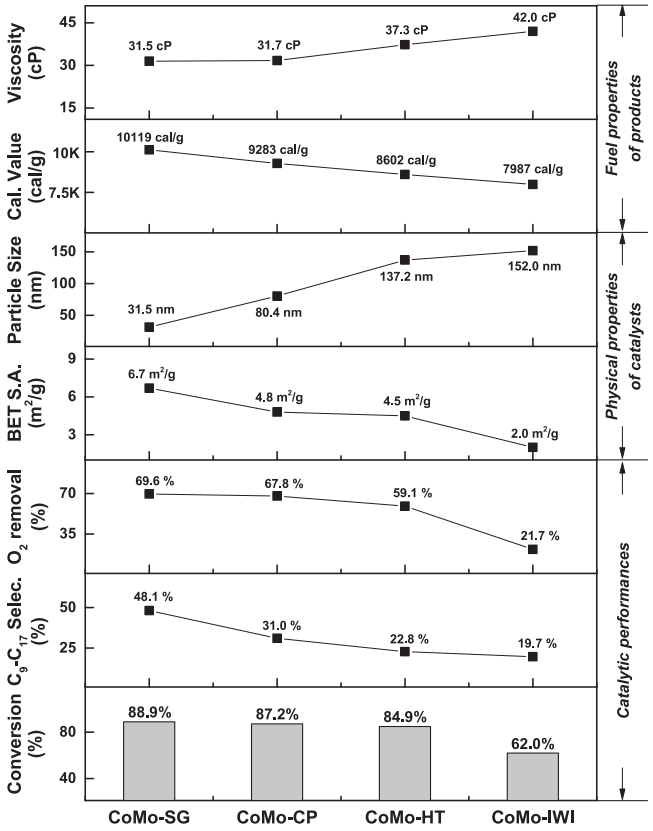

Fig. 13. The relationships between the physical properties of the catalysts, their catalytic performances, and the fuel properties of the resulting reaction products.

conditions. The CoMo-SG catalyst exhibited the highest oleic acid conversion as well as C_9–C_{17} selectivity and oxygen removal rate of all prepared catalysts. The superior catalytic performance of the CoMo-SG catalyst is mainly the result of its physical properties and unique chemical properties. The reaction proceeded primarily via decarboxylation, but decarbonylation also occurred. Moreover, the oxide $CoMoO_4$

species in the CoMo catalysts is the active species that drives the solvent-free catalytic deoxygenation of oleic acid. Analysis of the basic fuel properties of the resulting product revealed that it can be used as a biofuel for diesel engines. However, certain physical properties of the product were somewhat sub-optimal and must be improved before the biofuel can be used commercially. Overall, this study describes an efficient and accessible method for the production of biofuel for diesel engines. The support- and sulfide-free CoMo-SG catalyst described here exhibits significant promise as a catalyst for facile biofuel production via solvent-free catalytic deoxygenation of oleic acid.

Acknowledgments

This work was supported by the National Research Foundation of Korea (NRF) grant funded by the Korea government (MSIP) (NRF-2017R1A2B4007145). This research was supported by Changwon National University in 2018.

References

[1] A.P. Vyas, J.L. Verma, N. Subrahmanyam, A review on FAME production processes, Fuel 89 (2010) 1–9.
[2] M.E. Borges, L. Díaz, J. Gavín, A. Brito, Estimation of the content of fatty acid methyl esters (FAME) in biodiesel samples from dynamic viscosity measurements, Fuel Process. Technol. 92 (2011) 597–599.
[3] J.-O. Shim, D.-W. Jeong, W.-J. Jang, K.-W. Jeon, B.-H. Jeon, S.-H. Kim, H.-S. Roh, J.-G. Na, S.S. Han, C.H. Ko, Bio-diesel production from deoxygenation reaction over $Ce_{0.6}Zr_{0.4}O_2$ supported transition metal (Ni, Cu, Co, and Mo) catalysts, J. Nanosci. Nanotechnol. 16 (2016) 4587–4592.
[4] C. Kordulis, K. Bourikas, M. Gousi, E. Kordouli, A. Lycourghiotis, Development of nickel based catalysts for the transformation of natural triglycerides and related compounds into green diesel: a critical review, Appl. Catal. B: Environ. 181 (2016) 156–196.
[5] H.-S. Roh, I.-H. Eum, D.-W. Jeong, B.E. Yi, J.-G. Na, C.H. Ko, The effect of calcination temperature on the performance of $Ni/MgO–Al_2O_3$ catalysts for decarboxylation of oleic acid, Catal. Today 164 (2011) 457–460.
[6] J.-O. Shim, D.-W. Jeong, W.-J. Jang, K.-W. Jeon, B.-H. Jeon, S.Y. Cho, H.-S. Roh, J.-G. Na, C.H. Ko, Y.-K. Oh, S.S. Han, Deoxygenation of oleic acid over $Ce_{(1-x)}Zr_{(x)}O_2$ catalysts in hydrogen environment, Renew. Energy 65 (2014) 36–40.
[7] Z. Zhang, Q. Yang, H. Chen, K. Chen, X. Lu, P. Ouyang, J. Fu, J.G. Chen, In situ hydrogenation and decarboxylation of oleic acid into heptadecane over a Cu–Ni alloy catalyst using methanol as a hydrogen carrier, Green Chem. 20 (2018) 197–205.
[8] D. Otyuskaya, J.W. Thybaut, R. Lødeng, G.B. Marin, Anisole hydrotreatment kinetics on CoMo catalyst in the absence of sulfur: experimental investigation and model construction, Energy Fuels 31 (2017) 7082–7092.
[9] X. Zhao, L. Wei, S. Cheng, E. Kadis, Y. Cao, E. Boakye, Z. Gu, J. Julson, Hydroprocessing of carinata oil for hydrocarbon biofuel over $Mo-Zn/Al_2O_3$, Appl. Catal. B: Environ. 196 (2016) 41–49.
[10] K.-W. Jeon, J.-O. Shim, W.-J. Jang, D.-W. Lee, H.-S. Na, H.-M. Kim, Y.-L. Lee, S.-Y. Yoo, H.-S. Roh, B.-H. Jeon, J.W. Bae, C.H. Ko, Effect of calcination temperature on the association between free NiO species and catalytic activity of $Ni-Ce_{0.6}Zr_{0.4}O_2$ deoxygenation catalysts for biodiesel production, Renew. Energy 131 (2019) 144–151.
[11] Y. Liu, L. Yao, H. Xin, G. Wang, D. Li, C. Hu, The production of diesel-like hydrocarbons from palmitic acid over HZSM-22 supported nickel phosphide catalysts, Appl. Catal. B: Environ. 174 – 175 (2015) 504–514.
[12] S.P. Srivastava, J. Hancsók, Fuels and Fuel-Additives, first ed., John Wiley & Sons, Inc, New Jersey, 2014.
[13] X. Zhang, Essential scientific mapping of the value chain of thermochemically converted second-generation bio-fuels, Green Chem. 18 (2016) 5086–5117.
[14] W.M.A. Wan Mahmood, C. Theodoropoulos, M. Gonzalez-Miquel, Enhanced microalgal lipid extraction using bio-based solvents for sustainable biofuel production, Green Chem. 19 (2017) 5723–5733.
[15] L. Yang, B.W. McNichols, M. Davidson, B. Schweitzer, D.A. Gómez-Gualdrón, B.G. Trewyn, A. Sellinger, M.A. Carreon, Noble metal-free catalytic decarboxylation of oleic acid to n-heptadecane on nickel-based metal-organic frameworks (MOFs), Catal. Sci. Technol. 7 (2017) 3027–3035.
[16] J.G. Immer, M.J. Kelly, H.H. Lamb, Catalytic reaction pathways in liquid-phase deoxygenation of C18 free fatty acids, Appl. Catal. A Gen. 375 (2010) 134–139.
[17] M. Snåre, I. Kubičková, P. Mäki-Arvela, K. Eränen, D.Y. Murzin, Heterogeneous catalytic deoxygenation of stearic acid for production of biodiesel, Ind. Eng. Chem. Res. 45 (2006) 5708–5715.
[18] R.A. Sheldon, Green and sustainable manufacture of chemicals from biomass: state of the art, Green Chem. 16 (2014) 950–963.
[19] Y.-K. Oh, K.-R. Hwang, C. Kim, J.R. Kim, J.-S. Lee, Recent developments and key barriers to advanced biofuels: a short review, Bioresour. Technol. 257 (2018) 320–333.
[20] Q. Tian, K. Qiao, F. Zhou, K. Chen, T. Wang, J. Fu, X. Lu, P. Ouyang, Direct production of aviation fuel range hydrocarbons and aromatics from oleic acid without an added hydrogen donor, Energy Fuels 30 (2016) 7291–7297.
[21] J.-O. Shim, W.-J. Jang, K.-W. Jeon, D.-W. Lee, H.-S. Na, H.-M. Kim, Y.-L. Lee, S.-Y. Yoo, B.-H. Jeon, H.-S. Roh, C.H. Ko, Petroleum like biodiesel production by catalytic decarboxylation of oleic acid over $Pd/Ce-ZrO_2$ under solvent-free condition, Appl. Catal. A Gen. 563 (2018) 163–169.
[22] E. Santillan-Jimenez, T. Morgan, J. Lacny, S. Mohapatra, M. Crocker, Catalytic deoxygenation of triglycerides and fatty acids to hydrocarbons over carbon-supported nickel, Fuel 103 (2013) 1010–1017.
[23] B. Rozmysłowicz, P. Mäki-Arvela, A. Tokarev, A.-R. Leino, K. Eränen, D.Y. Murzin, Influence of hydrogen in catalytic deoxygenation of fatty acids and their derivatives over Pd/C, Ind. Eng. Chem. Res. 51 (2012) 8922–8927.
[24] L. Hermida, A.Z. Abdullah, A.R. Mohamed, Deoxygenation of fatty acid to produce diesel-like hydrocarbons: a review of process conditions, reaction kinetics and mechanism, Renew. Sustain. Energy. Rev. 42 (2015) 1223–1233.
[25] J.P. Ford, N. Thapaliya, M.J. Kelly, W.L. Roberts, H.H. Lamb, Semi-batch deoxygenation of canola- and lard-derived fatty acids to diesel-range hydrocarbons, Energy Fuels 27 (2013) 7489–7496.
[26] M. Arend, T. Nonnen, W.F. Hoelderich, J. Fischer, J. Groos, Catalytic deoxygenation of oleic acid in continuous gas flow for the production of diesel-like hydrocarbons, Appl. Catal. A Gen. 399 (2011) 198–204.
[27] M. Snåre, I. Kubičková, P. Mäki-Arvela, K. Eränen, J. Wärnå, D.Y. Murzin, Production of diesel fuel from renewable feeds: kinetics of ethyl stearate decarboxylation, Chem. Eng. J. 134 (2007) 29–34.
[28] Y. Wang, J. Wu, S. Wang, Hydrodeoxygenation of bio-oil over Pt-based supported catalysts: importance of mesopores and acidity of the support to compounds with different oxygen contents, RSC Adv. 3 (2013) 12635–12640.
[29] V.A. Yakovlev, S.A. Khromova, O.V. Sherstyuk, V.O. Dundich, D.Y. Ermakov, V.M. Novopashina, M. Yu, O. Lebedev, V.N. Bulavchenko, Parmon, Development of new catalytic systems for upgraded bio-fuels production from bio-crude-oil and biodiesel, Catal. Today 144 (2009) 362–366.
[30] E. Meller, U. Green, Z. Aizenshtat, Y. Sasson, Catalytic deoxygenation of castor oil over Pd/C for the production of cost effective biofuel, Fuel 133 (2014) 89–95.
[31] P. Mäki-Arvela, I. Kubičková, M. Snåre, K. Eränen, D.Y. Murzin, Catalytic deoxygenation of fatty acids and their derivatives, Energy Fuels 21 (2007) 30–41.
[32] S. Lestari, I. Simakova, A. Tokarev, P. Mäki-Arvela, K. Eränen, D.Y. Murzin, Synthesis of biodiesel via Deoxygenation of stearic acid over supported Pd/C catalyst, Catal. Lett. 122 (2008) 247–251.
[33] S. Lestari, P. Mäki-Arvela, K. Eränen, J. Beltramini, G.Q. Max Lu, D.Y. Murzin, Catalytic deoxygenation of stearic acid and palmitic acid in semibatch mode, Catal. Lett. 130 (2009) 48–51.
[34] I. Simakova, O. Simakova, P. Mäki-Arvela, A. Simakov, M. Estrada, D.Y. Murzin, Deoxygenation of palmitic and stearic acid over supported Pd catalysts: effect of metal dispersion, Appl. Catal. A Gen. 355 (2009) 100–108.
[35] S. Lestari, P. Mäki-Arvela, H. Bernas, O. Simakova, R. Sjöholm, J. Beltramini, G.Q. Max Lu, J. Myllyoja, I. Simakova, D.Y. Murzin, Catalytic deoxygenation of stearic acid in a continuous reactor over a mesoporous carbon-supported Pd catalyst, Energy Fuels 23 (2009) 3842–3845.
[36] I. Simakova, B. Rozmysłowicz, O. Simakova, P. Mäki-Arvela, A. Simakov, D.Y. Murzin, Catalytic deoxygenation of C18 fatty acids over mesoporous Pd/C catalyst for synthesis of biofuels, Top. Catal. 54 (2011) 460–466.
[37] R.G. Kukushkin, O.A. Bulavchenko, V.V. Kaichev, V.A. Yakovlev, Influence of Mo on catalytic activity of Ni-based catalysts in hydrodeoxygenation of esters, Appl. Catal. B: Environ. 163 (2015) 531–538.
[38] N.A. Grosso-Giordano, T.R. Eaton, Z. Bo, S. Yacob, C.-C. Yang, J.M. Notestein, Silica support modifications to enhance Pd-catalyzed deoxygenation of stearic acid, Appl. Catal. B: Environ. 192 (2016) 93–100.
[39] H. Xin, K. Guo, D. Li, H. Yang, C. Hu, Production of high-grade diesel from palmitic acid over activated carbon-supported nickel phosphide catalysts, Appl. Catal. B: Environ. 187 (2016) 375–385.
[40] A.E. Coumans, E.J.M. Hensen, A model compound (methyl oleate, oleic acid, triolein) study of triglycerides hydrodeoxygenation over alumina-supported NiMo sulfide, Appl. Catal. B: Environ. 201 (2017) 290–301.
[41] D. Sági, A. Holló, G. Varga, J. Hancsók, Co-hydrogenation of fatty acid by-products and different gas oil fractions, J. Clean. Prod. 161 (2017) 1352–1359.
[42] T. Szarvas, Z. Eller, T. Kasza, T. Ollár, P. Tétényi, J. Hancsók, Radioisotopic investigation of the oleic acid-1-^{14}C HDO reaction pathways on sulfided $Mo/P/Al_2O_3$ and NiW/Al_2O_3 catalysts, Appl. Catal. B: Environ. 165 (2015) 245–252.
[43] M. Peroni, G. Mancino, E. Baráth, O.Y. Gutiérrez, J.A. Lercher, Bulk and γ-Al_2O_3-supported Ni_2P and MoP for hydrodeoxygenation of palmitic acid, Appl. Catal. B: Environ. 180 (2016) 301–311.
[44] J.-O. Shim, D.-W. Jeong, W.-J. Jang, K.-W. Jeon, S.-H. Kim, B.-H. Jeon, H.-S. Roh, J.-G. Na, Y.-K. Oh, S.S. Han, C.H. Ko, Optimization of unsupported CoMo catalysts for decarboxylation of oleic acid, Catal. Commun. 67 (2015) 16–20.
[45] M. Krár, S. Kovács, D. Kalló, J. Hancsók, Fuel purpose hydrotreating of sunflower oil on $CoMo/Al_2O_3$ catalyst, Bioresour. Technol. 101 (2010) 9287–9293.
[46] K.A. Roger, Y. Zheng, Selective deoxygenation of biomass-derived bio-oils within hydrogen-modest environments: a review and new insights, ChemSusChem 9 (2016) 1750–1772.
[47] B.P. Pattanaik, R.D. Misra, Effect of reaction pathway and operating parameters on the deoxygenation of vegetable oils to produce diesel range hydrocarbon fuels: a review, Renew. Sustain. Energy Rev. 73 (2017) 545–557.
[48] R. Loe, E. Santillan-Jimenez, T. Morgan, L. Sewell, Y. Ji, S. Jones, M.A. Isaacs, A.F. Lee, M. Crocker, Effect of Cu and Sn promotion on the catalytic deoxygenation of model and algal lipids to fuel-like hydrocarbons over supported Ni catalysts, Appl. Catal. B: Environ. 191 (2016) 147–156.
[49] L. Di, S. Yao, S. Song, G. Wu, W. Dai, N. Guan, L. Li, Robust ruthenium catalysts for

the selective conversion of stearic acid to diesel-range alkanes, Appl. Catal. B: Environ. 201 (2017) 137–149.
[50] M. Arend, T. Nonnen, W.F. Hoelderich, J. Fischer, J. Groos, Catalytic deoxygenation of oleic acid in continuous gas flow for the production of diesel-like hydrocarbons, Appl. Catal. A Gen. 399 (2011) 198–204.
[51] Y. Liu, X. Yang, H. Liu, Y. Ye, Z. Wei, Nitrogen-doped mesoporous carbon supported Pt nanoparticles as a highly efficient catalyst for decarboxylation of saturated and unsaturated fatty acids to alkanes, Appl. Catal. B: Environ. 218 (2017) 679–689.
[52] B. Puértolas, T.C. Keller, S. Mitchell, J. Pérez-Ramírez, Deoxygenation of bio-oil over solid base catalysts: from model to realistic feeds, Appl. Catal. B: Environ. 184 (2016) 77–86.
[53] W. Li, Y. Gao, S. Yao, D. Ma, Yan N, Effective deoxygenation of fatty acids over Ni $(OAc)_2$ in the absence of H_2 and solvent, Green Chem. 17 (2015) 4198–4205.
[54] Q. Tian, Z. Zhang, F. Zhou, K. Chen, J. Fu, X. Lu, P. Ouyang, Role of solvent in catalytic conversion of oleic acid to aviation biofuels, Energy Fuels 31 (2017) 6163–6172.
[55] J.-G. Na, J.K. Han, Y.-K. Oh, J.-H. Park, T.S. Jung, S.S. Han, H.C. Yoon, S.H. Chung, J.-N. Kim, C.H. Ko, Decarboxylation of microalgal oil without hydrogen into hydrocarbon for the production of transportation fuel, Catal. Today 185 (2012) 313–317.
[56] W.-J. Jang, H.-M. Kim, J.-O. Shim, S.-Y. Yoo, K.-W. Jeon, H.-S. Na, Y.-L. Lee, D.-W. Jeong, J.W. Bae, I.W. Nah, H.-S. Roh, Key properties of Ni-MgO-CeO_2, Ni-MgO-ZrO_2, and Ni-MgO-$Ce_{(1-x)}Zr_{(x)}O_2$ catalysts for the reforming of methane with carbon dioxide, Green Chem. 20 (2018) 1621–1633.
[57] W.-J. Jang, Y.J. Hong, H.-M. Kim, J.-O. Shim, H.-S. Roh, Y.C. Kang, Alkali resistant Ni-loaded yolk-shell catalysts for direct internal reforming in molten carbonate fuel cells, J. Power Sources 352 (2017) 1–8.
[58] W.-J. Jang, H.-M. Kim, J.-O. Shim, S.-Y. Yoo, K.-W. Jeon, H.-S. Na, Y.-L. Lee, D.-W. Lee, H.-S. Roh, W.L. Yoon, Deactivation of SiO_2 supported Ni catalysts by structural change in the direct internal reforming reaction of molten carbonate fuel cell, Catal. Commun. 101 (2017) 44–47.
[59] J.-O. Shim, Y.J. Hong, H.-S. Na, W.-J. Jang, Y.C. Kang, H.-S. Roh, Highly active and stable Pt loaded $Ce_{0.75}Zr_{0.25}O_2$ yolk-shell catalyst for water-gas shift reaction, ACS Appl. Mater. Interfaces 8 (2016) 17239–17244.
[60] R. Ramkumar, M. Minakshi, Fabrication of ultrathin $CoMoO_4$ nanosheets modified with chitosan and their improved performance in energy storage device, Dalton Trans. 44 (2015) 6158–6168.
[61] G.K. Veerasubramani, K. Krishnamoorthy, S.J. Kim, Improved electrochemical performances of binder-free $CoMoO_4$ nanoplate arrays@Ni foam electrode using redox additive electrolyte, J. Power Sources 306 (2016) 378–386.
[62] M. Høj, D.K. Pham, M. Brorson, L. Mädler, A.D. Jensen, J.-D. Grunwaldt, Two-nozzle flame spray pyrolysis (FSP) synthesis of $CoMo/Al_2O_3$ hydrotreating catalysts, Catal. Lett. 143 (2013) 386–394.
[63] D. Zagorac, J.C. Schön, M. Rosić, J. Zagorac, D. Jordanov, J. Luković, B. Matović, Theoretical and experimental study of structural phases in $CoMoO_4$, Cryst. Res. Technol. 52 (2017) 1700069.
[64] T. Ono, N. Ogata, Y. Miyaryo, Characteristic features of Raman band shifts of scheelite-type molybdate catalysts exchanged with the ^{18}O tracer via redox reactions, J. Catal. 161 (1996) 78–86.
[65] M.Q. Yu, L.X. Jiang, H.G. Yang, Ultrathin nanosheets constructed $CoMoO_4$ porous flowers with high activity for electrocatalytic oxygen evolution, Chem. Commun. 51 (2015) 14361–14364.
[66] Z. Gu, R. Wang, H. Nan, B. Geng, X. Zhang, Construction of unique $Co3O_4$@$CoMoO_4$ core/shell nanowire arrays on Ni foam by the action exchange method for high-performance supercapacitors, J. Mater. Chem. A Mater. Energy Sustain. 3 (2015) 14578–14584.
[67] X. Yan, L. Tian, S. Atkins, Y. Liu, J. Murowchick, X. Chen, Converting CoMoO4 into CoO/MoO_x for overall water splitting by hydrogenation, ACS Sustain. Chem. Eng. 4 (2016) 3743–3749.
[68] Z. Yang, R. Li, Z. Deng, A deep study of the protection of Lithium cobalt Oxide with polymer surface modification at 4.5V high voltage, Sci. Rep. 8 (2018) 863.
[69] Z.-S. Jiang, Y.-H. Zhao, C.-F. Huang, Y.-H. Song, D.-P. Li, Z.-T. Liu, Z.-W. Liu, Metal-support interactions regulated via carbon coating – a case study of Co/SiO_2 for Fischer-Tropsch synthesis, Fuel 226 (2018) 213–220.
[70] M.A. Bica de Moraes, B.C. Trasferetti, F.P. Rouxinol, R. Landers, S.F. Durrant, J. Scarmínio, A. Urbano, Molybdenum oxide thin films obtained by the hot-filament metal oxide deposition technique, Chem. Mater. 16 (2004) 513–520.
[71] C. Ranga, R. Lødeng, V.I. Alexiadis, T. Rajkhowa, H. Bjørkan, S. Chytil, I.H. Svenum, J. Walmsley, C. Detavernier, H. Poelman, P. Van Der Voort, J.W. Thybaut, Effect of composition and preparation of supported MoO_3 catalysts for anisole hydrodeoxygenation, Chem. Eng. J. 335 (2018) 120–132.
[72] F. Xie, W.C.H. Choy, C. Wang, X. Li, S. Zhang, J. Hou, Low-temperature solution-processed hydrogen molybdenum and vanadium bronzes for an efficient hole-transport layer in organic electronics, Adv. Mater. 25 (2013) 2051–2055.
[73] Z. Yue, L. Li, J. Zhou, H. Zhang, Z. Gui, Preparation and characterization of NiCuZn ferrite nanocrystalline powders by auto-combustion of nitrate–citrate gels, Mater. Sci. Eng. B 25 (2013) 2051–2055.
[74] V. Subramanian, D.-W. Jeong, W.-B. Han, W.-J. Jang, J.-O. Shim, H.-S. Roh, H_2 production from high temperature shift of the simulated waste derived synthesis gas over magnetite catalysts prepared by citric acid assisted direct synthesis method, Int. J. Hydrogen Energy 38 (2013) 8699–8703.
[75] B. Peng, X. Yuan, C. Zhao, J.A. Lercher, Stabilizing catalytic pathways via redundancy: selective reduction of microalgae oil to alkanes, J. Am. Chem. Soc. 134 (2012) 9400–9405.
[76] B. Peng, C. Zhao, S. Kasakov, S. Foraita, J.A. Lercher, Manipulating catalytic pathways: deoxygenation of palmitic acid on multifunctional catalysts, Chem. Eur. J. 19 (2013) 4732–4741.
[77] S.C.A. de Almeida, C.R. Belchior, M.V.G. Nascimento, L.S.R. Vieira, G. Fleury, Performance of a diesel generator fuelled with palm oil, Fuel 81 (2002) 2097–2102.
[78] X.-Y. Li, R. Shang, M.-C. Fu, Y. Fu, Conversion of biomass-derived fatty acids and derivatives into hydrocarbons using a metal-free hydrodeoxygenation process, Green Chem. 17 (2015) 2790–2793.
[79] C. Zhao, T. Brück, J.A. Lercher, Catalytic deoxygenation of microalgae oil to green hydrocarbons, Green Chem. 15 (2013) 1720–1739.
[80] S. Xing, P. Lv, H. Yuan, L. Yang, Z. Wang, Z. Yuan, Y. Chen, Insight into forced hydrogen re-arrangement and altered reaction pathways in a protocol for CO_2 catalytic processing of oleic acid into C_8–C_{15} alkanes, Green Chem. 19 (2017) 4157–4168.
[81] H. Hazar, H. Aydin, Performance and emission evaluation of a CI engine fueled with preheated raw rapeseed oil (RRO)–diesel blends, Appl. Energy 87 (2010) 786–790.
[82] H. Raheman, A.G. Phadatare, Diesel engine emissions and performance from blends of karanja methyl ester and diesel, Biomass Bioenerg. 27 (2004) 393–397.
[83] M. Gumus, S. Kasifoglu, Performance and emission evaluation of a compression ignition engine using a biodiesel (apricot seed kernel oil methyl ester) and its blends with diesel fuel, Biomass Bioenerg. 34 (2010) 134–139.
[84] O.M.I. Nwafor, Effect of advanced injection timing on emission characteristics of diesel engine running on natural gas, Renew. Energy 32 (2007) 2361–2368.